JOURNAL OF ADVANCED MECHANICAL ENGINEERING APPLICATIONS
e-ISSN: 2716-6201

JAMEA

Vol. 6 No. 2 (2025) 83-90
https://publisher.uthm.edu.my/ojs/index.php/jamea

A Pilot Study of a Lumped Parameter Model on the Middle Cerebral Artery for Hemodynamic Parameters Assessment

Nurul Syazana Qhairunnessa Salleh[1], Nabilah Ibrahim[1]*, Nur'Afifah Yousri[1] Ishkrizat Taib[2], Shahnoor Shanta[3]

[1] *Faculty of Electrical and Electronic Engineering, Universiti Tun Hussein Onn Malaysia, 86400 Batu Pahat, Johor, MALAYSIA*
[2] *Faculty of Mechanical and Manufacturing Engineering, Universiti Tun Hussein Onn Malaysia, 86400 Batu Pahat, Johor, MALAYSIA*
[3] *Department of Computer and Information Sciences, Harrisburg University of Science and Technology, PA, USA*

*Corresponding Author: nabilah@uthm.edu.my
DOI: https://doi.org/10.30880/jamea.2025.06.02.008

Article Info

Received: 8 June 2025
Accepted: 24 September 2025
Available online: 31 December 2025

Keywords

Middle cerebral artery, computational fluid dynamics, lumped parameter models, hemodynamic, wall shear stress, pressure distribution

Abstract

The middle cerebral artery (MCA), especially the M1 and M2 segments, is critical in cerebrovascular health. Conventional imaging techniques for assessing atherosclerosis have limitations in accurately estimating boundary conditions for computational fluid dynamics (CFD) simulations. This initial study addresses these limitations by employing lumped parameter models (LPMs) to derive more precise boundary conditions for CFD simulations of blood flow in the MCA. The goal is to improve the accuracy of CFD models by integrating dynamic parameters such as resistance and compliance, which are essential for understanding localized hemodynamic changes due to atherosclerosis. The early stage highlighted the simulation of cerebral blood flow with LPMs, analyzing hemodynamic factors such as wall shear stress (WSS), pressure distribution, and flow rate, and visualizing these effects in the MCA. The data geometry for boundary condition setup in CFD simulation was calculated for the blood density of 1060 kg/m^3, blood viscosity of 0.0035 Pa.s, length of M1 at 19.64 mm, diameter of M1 at 2.66 mm, length of L2 at 13.5 mm, and diameter of M2 at 2.4 mm. In addition to that, the calculated value of electrical components was also presented. Using CFD and LPMs, this study offers the preparation of parameter setups for analyzing the deeper mechanism of atherosclerosis alteration in cerebral circulation, potentially enhancing diagnostic accuracy and treatment strategies for stroke prevention.

1. Introduction

Atherosclerosis significantly contributes to the burden of ischemic stroke, accounting for nearly 50% of cases [1][2]. The presence of atherosclerotic plaques in cerebral arteries can lead to severe complications, including permanent brain damage and even death if left untreated. The middle cerebral artery (MCA) is a vital blood vessel supplying a significant portion of the lateral surface of the brain, including areas critical for motor and sensory functions [3]. It is divided into two segments: the M1 (horizontal) and M2 (insular) segments, which are particularly crucial in cerebrovascular health and the impact of atherosclerosis [4]. Anatomically, the M1 segment

starts at the origin of the MCA at the bifurcation of the ICA and travels laterally, posterior to the sphenoid ridge, and terminates at the genu, which is the junction of the sphenoidal and operculo-insular compartments of the Sylvian fissure [5]. Bifurcation of the MCA occurred proximally in 86% of the hemispheres studied [5]. The M2 segment continues from the genu, crossing the limen insulae, and terminating at the circular sulcus of the insula. Atherosclerosis significantly affects both the M1 and M2 segments of the MCA, with plaque formation commonly occurring at the bifurcation point where the M1 transitions into the M2 segment [6].

The integration of lumped parameter modelling with computational fluid dynamics (CFD) represents a synergistic approach to studying cerebral circulation. While the method provides a detailed and accurate representation of blood flow dynamics by simulating the complex fluid mechanics within three-dimensional vascular geometries, lumped parameter models offer a complementary and computationally efficient approach. This approach enables the study of how these parameters interact within the cerebral circulation, which is crucial given the complex nature of blood flow dynamics in this region.

This pilot study addresses the critical need for accurate estimation of boundary conditions in computational fluid dynamics (CFD) analyses of cerebral artery blood flow, particularly concerning the M1 and M2 segments of the MCA. Atherosclerosis impacts hemodynamics by altering arterial compliance and resistance, often leading to plaque formation in regions with disturbed blood flow. However, existing CFD studies frequently rely on generalized or simplified boundary conditions, potentially compromising the reliability of their simulations. Therefore, this study proposes to fill this gap by employing lumped parameter models (LPMs) for estimating boundary conditions of the M1 and M2 segments. LPMs excel at simulating dynamic responses to changes in blood flow and pressure by incorporating time-dependent variations in parameters [7]. Similar work has been presented, with mean errors < 7% [8]. Furthermore, [9] proposed an LPM approach based on the actual length of the vessel to improve the pressure and flow rate values. The capability of LPM is essential for understanding the atherosclerosis effects on both steady-state and transient hemodynamics [10]. By integrating LPMs with CFD, this study enables more detailed investigations of localized atherosclerotic effects, such as wall shear stress and flow patterns around stenoses. Through accurate mapping of the distal vascular elements of the MCA, this study seeks to improve the precision of CFD simulations, thereby advancing an understanding of hemodynamic alterations associated with atherosclerosis and their impact on cerebrovascular health.

2. Methodology

2.1 Simulation Design for the Middle Cerebral Artery (MCA)

The first phase of preprocessing begins with the development of a schematic diagram of the M1 and M2 segments of the MCA. This initial step is developed for accurately capturing the geometry of the artery. Later, data is collected to inform the geometry, ensuring precise lengths and dimensions for the MCA segments. This information is vital for creating a simplified 3D model, which is then refined using CAD software to accurately represent the anatomical features of the artery. The simplified model of the cerebral artery is simulated using CFD techniques to analyze blood flow dynamics. Next, a discretization technique is applied to prepare the models for computational fluid dynamics (CFD) simulation. This process involved two key steps, which are meshing and defining governing equations. The meshing process involves dividing the continuous geometry into smaller, manageable elements or meshes, which are essential for numerical analysis. A mesh generator is employed to create these meshes, ensuring they are sufficiently fine to capture the complexities of blood flow while maintaining computational efficiency. The assessment of mesh quality is necessary to obtain accurate simulation results, as it includes a decision point to determine whether the Grid Independence Test (GIT) has been sufficiently refined. The governing equations for Newtonian blood flow are established, incorporating essential parameters. Here, an inlet velocity profile and boundary conditions, including a no-slip condition at arterial walls for modeling viscous effects, are defined. Incompressibility is assumed due to the low speed and constant density of blood flow. Model properties and boundary conditions (inlet, wall, outlet) are defined for the M1 and M2 segments with blood density and viscosity set at 1060 kg/m^3 and 0.0035 Pa, respectively. This step of setting up the model concludes the preprocessing phase before transitioning to the processing stage.

Fig. 1 depicts a 3D model and a 3D mesh model of an intracranial diverter, developed utilizing ANSYS software. The model provides a simplified representation, emphasizing the key anatomical features of the M1 and M2 segments. Meanwhile, the mesh consists of tetrahedral elements along the 3D shapes with four triangular faces, functioning to efficiently fill 3D space. The mesh density is relatively uniform throughout the model with no apparent regions of excessive refinement or coarseness. The elements are well-shaped, exhibiting minimal skewness.

J. of Advanced Mechanical Engineering Applications Vol. 6 No. 2 (2025) p. 83-90

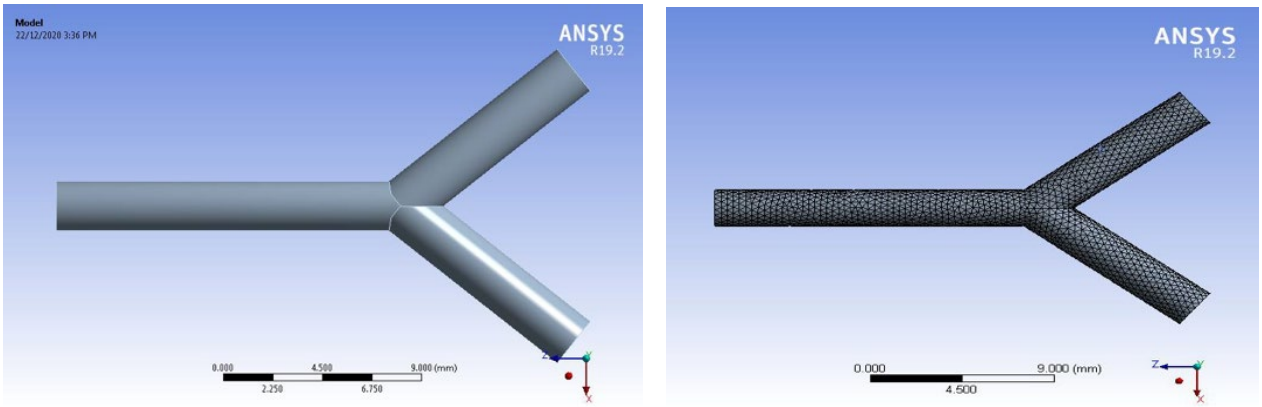

Fig. 1 *Intracranial diverter design using ANSYS in simplified 3D model (left) and 3D mesh model (right)*

2.2 The concept of a lumped parameter model

This study focused on the 3D lumped parameter model as the main mathematical modeling, where the values of the resistor, capacitor, and inductor are derived from the blood vessel's properties on a per unit length basis. Fig. 2 shows the intracranial diverter comprising the M1 and M2 segments that are modeled as an electrical circuit. The M1 segment, the initial portion of the diverter, is represented by a resistor (*R1*) and an inductor (*L1*) in series. The M2 segment, which bifurcates into two branches, is similarly modelled. A resistor (*R2*) and an inductor (*L2*) represented the resistance and inertia within the M2 segment before the bifurcation. The bifurcation itself is represented by the division of the circuit into two parallel paths. Each branch of the M2 segment is modeled as a terminal load. These terminal loads typically consist of a resistor (*RL1*, *RL3*) representing the resistance to blood flow within the branch. Meanwhile, a capacitor (*CL1*, *CL2*) represents the compliance of the vessel wall. Compliance refers to the ability of the vessel to expand and store blood. The flow of blood entering the M1 segment is represented by *q1*, while the flow entering the M2 segment is represented by *q2*.

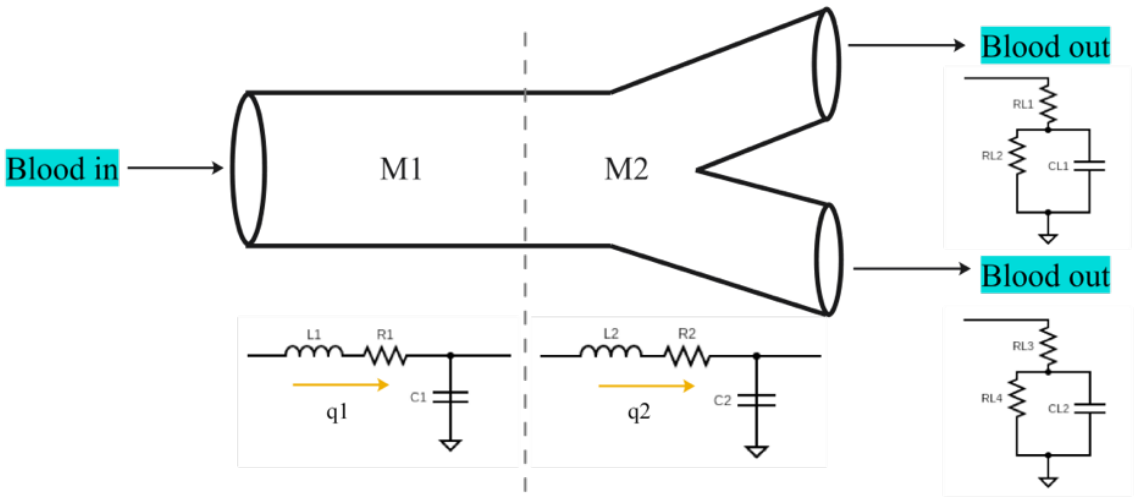

Fig. 2 *Intracranial diverter with electrical components equivalent*

Fig. 3 depicts an electrical schematic of a circuit representing the M1 and M2 arterial segments. The M2 segment bifurcates into branches designated M2a and M2b, with each branch modeled as a terminal load. This configuration suggested a bifurcating structure with inherent resistance within each branch, contributing to the overall load.

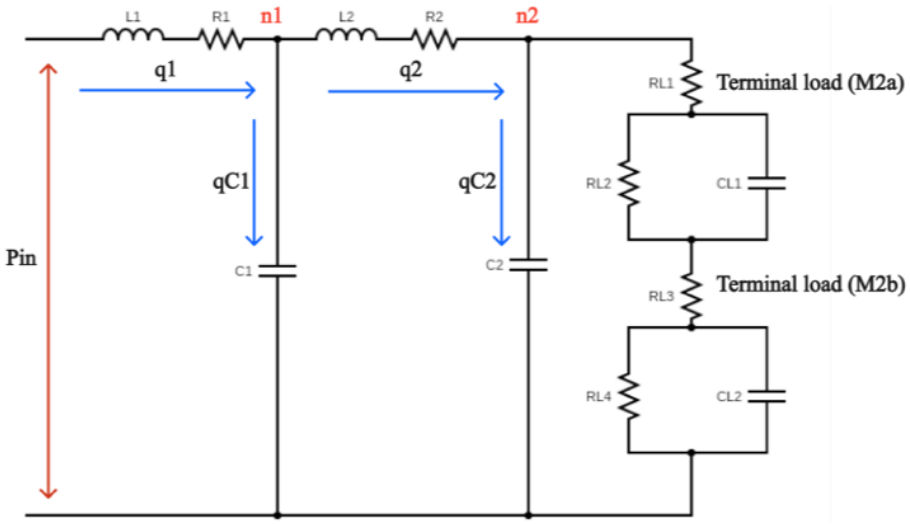

Fig. 3 *Electrical schematic of model for blood flow*

Equation (1) specifies the resistance for each discrete resistor in this discretized model, where R is expressed in Ns/m^5.

$$R = \ell R_{viscous} = C_v \frac{8\mu\ell}{\pi r4} \tag{1}$$

The inductance in each discrete inductor element is formulated as in equation (2), with units of Ns^2/m^5.

$$L = \ell \mathrm{L} = C_u \frac{\rho\ell}{\pi r^2} \tag{2}$$

Since the capacitance in this circuit is represented as the compliance of the arteries that is pressure-dependent, the following equation is expressed with SI units of m^5/N.

$$C = \frac{q}{dP/dt} \tag{3}$$

Here, the μ represents the blood viscosity and ρ represents the blood density. Meanwhile, in the circuit analysis, a node is the junction of two or more circuit elements. Fig. 3 labels the nodes as n1 (node 1) and n2 (node 2), indicating different segments of M1 and M2. This model treats each grouping of a resistor, inductor, and capacitor as a unified element, establishing a node where these components connect. Based on this, the initial element receives an input flow labeled *q1*, and an input pressure designated P_{in}. Subsequently, the flow leaving node 1 towards the capacitor is identified as *qC1*, accompanied by pressure *P1*.

As the first-order differential equation is established at node 1, the pressure drops across the initial resistor and inductor, as expressed in Equation (4).

$$P_{in} - \mathrm{P1} = q1R1 + L_1 \frac{\mathrm{d}q1}{dt} \tag{4}$$

In this context, P_{in} is the input pressure, *P1* is the pressure at node 1, and q indicates the arterial flow. The time rate of change of flow is designated dq/dt. The flow into the capacitor at node 1 is described by a second differential equation. Here, *q1* equals the vessel compliance $C1$ times dP/dt.

$$qC1 = C_{v1} \frac{\mathrm{dP1}}{dt} \tag{5}$$

Since P and q depend on time and location, and time is the independent variable, this model facilitates understanding the flow-pressure relationship. The system of two first-order differential equations can be derived independently for each node. This results in a final model with 2n first-order ordinary differential equations, with two equations for each node (node 1 through node n). The two equations for node 2, for example, are presented as follows:

$$P1 - \mathrm{P2} = q2R2 + L_2 \frac{\mathrm{d}q2}{dt} \quad (6)$$

$$qC2 = C_{v2} \frac{\mathrm{dP2}}{dt} \quad (7)$$

In order to mitigate the complexity and computational cost associated with individually modelling the M1 and M2 segments, the modelling system is lumped together. A terminal load is introduced, consisting of a resistor in series with a parallel combination of a second resistor and a capacitor, as shown in Figure 4.

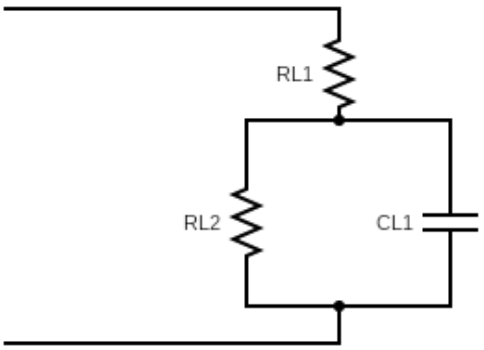

Fig. 4 *Terminal load of the model*

The total terminal resistance is determined by summing the two resistors. Under the steady-state conditions, capacitors behave as open circuits, as all voltages and currents are constant. Therefore, capacitors are neglected, and the total impedance is equivalent to the total load resistance, as expressed in equation (8).

$$ZT = R1 + R2 \quad (8)$$

2.3 Hemodynamic Parameter Setup

This study focused on Wall Shear Stress (WSS), pressure distribution, and flow rate. The ranges for those parameters are summarized in Table 1. In a healthy artery, WSS typically ranges from 1 to 7 Pa, with a common mean value of approximately 1.5 Pa [11] [12]. Low shear stress is defined as values below 1 Pa, which is linked to an increased risk of atherosclerosis and plaque formation. In this study, the WSS range is setup between 0.5 Pa and 1.5 Pa, with 0.5 Pa considering athero-prone cases. Normal pressure gradients in healthy arteries are usually less than 15 mmHg [13], indicating smooth blood flow without significant obstructions. In contrast, regions affected by stenosis due to atherosclerosis may exhibit pressure gradients exceeding 15 mmHg with significant narrowing and increased resistance that can lead to reduced blood flow and ischemia. The average cardiac output is 5 L/min [13], which results in varying flow rates across different segments of the vascular system. In areas affected by atherosclerosis, flow rates can significantly decrease due to the increased resistance from plaque buildup. This reduction in flow may lead to symptoms such as claudication or, in severe cases, critical limb ischemia.

Table 1 *The range parameters set up to observe the results of the wall on cerebral arteries*

Parameter	Range	Consequence
Wall Shear Stress (WSS)	0.5 Pa ≤ _WSS ≤ _1.5 Pa	Low WSS increases plaque formation, and high WSS leads to plaque rupture.
Pressure distribution (P)	P ≥ 15mmHg	Arterial narrowing
Flow rate (F)	F ≤ 5L/min	Plaque buildup

3. Parameters, Results, and Discussion

The M1 segment, the initial and straight portion of the diverter, was considered as a cylindrical tube extending from the left side of the image. The M2 segment, characterized by its bifurcation, branches off from the M1 segment, forming two distinct pathways. In this designation, the point of bifurcation where the M1 segment was divided into the two M2 branches is clearly discernible. The model utilized simplified geometries and cylinders as a way to reduce computational complexity in subsequent CFD simulations. Fine details, such as surface textures

or irregularities on the vessel walls, were omitted for simplicity. This 3D model was able to serve as the basis for CFD simulations to study the blood flow characteristics within the diverter, including velocity, pressure, and shear stress distributions.

In addition to this pilot study, the parameter value of resistance, capacitance, and inductance were calculated. These calculated results serve as the boundary conditions for CFD simulations. Here, the circuit model is considered a turbulent, incompressible, no-slip condition at the wall and in a steady state. The parameters settings and the data geometry of M1 and M2 are shown in Table 2.

Table 2 *The parameter setup and geometry*

Parameter	Calculated Value	Clinical Value
Blood density (ρ)	1060 kg/m^3	-
Blood viscosity (μ)	0.0035 Pa.s	-
Length of M1 (L1)	19.64 mm	24.1 mm [14], 15.62 [15]
Diameter of M1 (D1)	2.66 mm	3.1 mm [14], 2.23 mm [15]
Length of M2 (L2)	13.5 mm	-
Diameter of M2 (D2)	2.4 mm	-

Meanwhile, under the steady-state conditions, flow rates and pressures remain constant, thus resulting in a zero-time derivative. The model development employed Kirchhoff's Voltage Law (KVL) and Kirchhoff's Current Law (KCL), with the fundamental principles governing circuit behavior. Table 3 presents the results for each component in the electrical model. The values would be employed in the later finding of blood flow velocity and blood pressure profile.

Table 3 *The results of parameters for the intracranial diverter model*

Component	Parameter	Value
M1 segment	R1	$1.5 \times 10^8\ Pa.s/m^3$
M1 segment	L1	$1.4 \times 10^4\ kg/m^4$
M1 segment	C1	$1 \times 10^{-10}\ m^3/Pa$
M2 segment	R2	$2.2 \times 10^8\ Pa.s/m^3$
M2 segment	L2	$9.4 \times 10^8\ kg/m^4$
M2 segment	C2	$1 \times 10^{-10}\ m^3/Pa$
Terminal load (M2a)	RL1	$1.5 \times 10^8\ Pa.s/m^3$
Terminal load (M2a)	RL2	$1.5 \times 10^8\ Pa.s/m^3$
Terminal load (M2b)	RL3	$2.0 \times 10^8\ Pa.s/m^3$
Terminal load (M2b)	RL4	$2.0 \times 10^8\ Pa.s/m^3$

Since the flow is turbulent, the Hagen-Poiseuille equation was employed as the starting point to calculate the value of resistance. It provides a relationship between pressure drop, flow rate, viscosity, and vessel geometry. Furthermore, the Darcy-Weisbach equation was employed to account for the additional pressure losses due to turbulence. Once the Reynolds number is calculated, the friction factor can be determined; thus, the pressure drop and resistance can be estimated. The general equation to estimate the Reynolds number is shown in Equation (9), and the result of these calculations is summarized in Table 4.

$$Re = (pvD)/\mu \tag{9}$$

Table 4 *Calculated Reynolds number*

Inlet velocity	Segment	Value
0.31 m/s	M1	251
	M2	215
1.42 m/s	M1	1135
	M2	1021

Here, the Reynolds number calculations revealed the distinct flow regimes within the intracranial diverter model based on the inlet velocity. For the lower inlet velocity (0.31 m/s), the Reynolds numbers in both the M1 and M2 segments fell below the critical value, indicating laminar flow. In contrast, for the higher inlet velocity (1.42 m/s), the Reynolds numbers in both segments significantly exceeded, indicating turbulent flow conditions. These findings have implications for the selection of numerical methods employed in subsequent CFD simulations. In the laminar flow scenario (0.31 m/s), standard CFD solvers with appropriate boundary conditions can be utilized to capture the fluid dynamics within the diverter. However, for the turbulent flow scenario (1.42 m/s), the use of turbulence models is imperative to accurately represent the complex flow characteristics associated with turbulent flow.

Later, considering the laminar flow and healthy conditions [16], an inlet velocity of 0.45 m/s is decided. Three levels of stenosis are set up with the buildup of plaque of 25%, 50%, and 75%. Those plaque thicknesses are calculated based on the plaque percentage to the arterial diameter. The following Table 5 shows the summary.

Table 5 *Simplified models of the M1 segment based on stenosis level*

Percentage Atherosclerosis	Simplified model of M1 segment	Plaque thickness (mm)
25%		0.65
50%		1.30
75%		1.95

Even for the cases where the overall flow is expected to be laminar, employing CFD simulations with turbulence models is advisable. Turbulence models, such as the k-ω SST model, can capture small-scale flow features and transient phenomena that might not be accurately predicted by laminar flow solvers. The k-ω SST model, renowned for its versatility, can handle both laminar and turbulent flow regimes, making it suitable for a broad range of flow conditions. While the Reynolds number calculations provide initial insights into the flow regime, it is crucial to acknowledge that the simplified assumptions underlying the model may not fully capture the intricate flow behavior within the diverter.

Therefore, it is prudent to employ CFD simulations with appropriate turbulence models even for the lower inlet velocity to investigate the potential for localized turbulence or transient flow phenomena. By incorporating turbulence modeling and refining the CFD model with more realistic geometric and physiological parameters, it is possible to gain a more comprehensive and accurate understanding of the flow dynamics in the intracranial diverter and its implications for clinical applications. This pilot analysis illustrates the value of considering the Reynolds number and employing suitable CFD techniques to accurately capture the complex flow characteristics within the intracranial diverter model.

4. Conclusion

CFD simulations that are combined with augmented LPMs have demonstrated an alternative method in modeling cerebral blood flow within the middle cerebral artery (MCA) that specifically focuses on the M1 and M2 segments. This approach refines CFD simulations by providing more precise boundary conditions and overcoming the limitations of current imaging techniques. This enhancement enables the analysis of hemodynamic factors of wall shear stress, pressure distribution, and flow rate. Moreover, CFD models have emerged as valuable tools for understanding the complex hemodynamics of blood flow within the human body. The presence of these plaques can significantly disrupt blood flow, leading to localized changes in hemodynamic parameters with crucial implications for cerebrovascular health. In conclusion, the integration of LPMs with CFD represents a significant advancement in the field of computational hemodynamics. By providing detailed simulations of blood flow within the cerebrovascular system, these models offer invaluable insights into the impact of atherosclerosis on cerebral blood flow. This enhanced understanding has the potential to revolutionize the diagnosis and treatment of cerebrovascular diseases, ultimately leading to improved patient outcomes.

Acknowledgement

This research was supported by Universiti Tun Hussein Onn Malaysia through Multidisciplinary Research Grant MDR (votQ688).

Conflict of Interest

The authors declare that there is no conflict of interest regarding the publication of the paper.

Author Contribution

The authors confirm contribution to the paper as follows: ***simulation design:*** *Nurul Syazana Qhairunnesa;* ***data collection:*** *Nurul Syazana Qhairunnesa, Nur'Afifah Yousri;* ***analysis and interpretation of results:*** *Nurul Syazana Qhairunnesa;* ***draft manuscript preparation:*** *Nurul Syazana Qhairunnesa, Nabilah Ibrahim, Ishkrizat Taib, Shahnoor Shanta. All authors reviewed the results and approved the final version of the manuscript.*

References

[1] Q. Kong, X. Ma, L. Li, C. Wang, X. Du, and Y. Wan (2023). Atherosclerosis Burden of Brain- and Heart-Supplying Arteries and the Relationship with Vascular Risk in Patients with Ischeminc Stroke. *J American Heart Assoc 12, 1-10.*

[2] V.L. Feigin, B.A. Stark, C.O. Johnson, G.A. Roth, C. Bisignano, G.G. Abady, M. Abbasifard, M. Abbasi-Kangevari, F. Abd-Allah, V. Abedi (2021). Global, regional, and national burden of stroke and its risk factors in 1990–2019: A systematic analysis for the global burden of disease study 2019. *The Lancet Neurology 20*, 795–820.

[3] A. Nouh, J. Remke, and S. Ruland (2014). Ischemic posterior circulation stroke: a review of anatomy, clinical presentations, diagnosis, and current management. *Frontiers in Neurology 5*, 1-16.

[4] S. Bek, T. Kasikci, G. Genc, S. Demirkaya, and Z. Odabaşi (2009). Vasomotor properties of the M2 segment of the middle cerebral artery. *J Neurology 257*, 556–562.

[5] V. Zwan, B. Hillen, C.A. Tulleken, M. Dujovny (1992). Variability of the territories of the major cerebral arteries. *Journal of Neurosurgery 77*, 927-940.

[6] G. Nakazawa (2010). Pathological Findings at Bifurcation Lesions: The Impact of Flow Distribution on Atherosclerosis and Arterial Healing after Stent Implantation. *J American College of Cardiology 55*, 1679-1687.

[7] D.S. Liebeskind (2015). Noninvasive fractional flow on MRA predicts stroke risk of intracranial stenosis. *J Neuroimaging 25*, 87–91.

[8] M. Mirramezani, S. C. Shadden (2020). A distributed lumped parameter model of blood flow. *Ann Biomed Eng* 48, 2870 – 2886.

[9] V. Milisic, A. Quarteroni (2004) Analysis of lumped parameter models for blood flow simulations and their relation with 1D models: *Mathematical Modelling and Numerical Analysis 38*, 613-632.

[10] A.I. Qureshi, E. Feldmann, C.R. Gomez, S.C. Johnston, S.E. Kasner, D.C. Quick, and O.O. Zaidat (2009). Intracranial atherosclerotic disease: an update. *Annals of Neurology 66*, 730–738.

[11] G. Kahilogullari, H.C. Ugur, A. Comert, I. Tekdemir, and Y. Kanpolat (2012). The branching pattern of the middle cerebral artery: Is the intermediate trunk real or not? An anatomical study correlating with simple angiography. *J Neurosurgery 116,* 1024–1034.

[12] S.V. Marinkovic, M.S. Kovacevic, and J.M. Marinkovic (1985). Perforating branches of the middle cerebral artery: Microsurgical anatomy of their extracerebral segments. *Journal of Neurosurgery 63,* 266–271.

[13] M. Żyliński (2015). Individualization of the parameters of the three-elements Windkessel model using the carotid pulse signal. *Photonics Applications in Astronomy, Communications, Industry, and High-Energy Physics Experiments 9662*, 96621N.

[14] N. Papazova, A. Velkova, N. Lazarov (2009). Anatomical features of middle cerebral artery. *Folia Medica 51*, 20-23.

[15] A. Zurada, J. Gielecki, R. S. Tubbs, M. Loukas, W. Maksymowics (2011). Three-dimensional morphometrical analysis of the M1 segment of the middle cerebral artery: Potential clinical and neurosurgical implications. *Clinical Anatomy 24,* 34-41.

[16] Y. Zhang, C. Kleinstreuer (2003). Effects of the inlet conditions and blood models on accurate simulation of blood flow in a patient-specific cerebral aneurysm. AIP Advances 5, 057209.